JACS
JOURNAL OF THE AMERICAN CHEMICAL SOCIETY
Article
pubs.acs.org/JACS

A Hafnium-Based Metal–Organic Framework as a Nature-Inspired Tandem Reaction Catalyst

M. Hassan Beyzavi,[†] Nicolaas A. Vermeulen,[†] Ashlee J. Howarth,[†] Samat Tussupbayev,[‡] Aaron B. League,[‡] Neil M. Schweitzer,[†] James R. Gallagher,[§] Ana E. Platero-Prats,[⊥] Nema Hafezi,[†] Amy A. Sarjeant,[†] Jeffrey T. Miller,[§,∥] Karena W. Chapman,[⊥] J. Fraser Stoddart,[*,†] Christopher J. Cramer,[*,‡] Joseph T. Hupp,[*,†] and Omar K. Farha[*,†,#]

[†]International Institute for Nanotechnology (IIN) and Center for the Chemistry of Integrated Systems (CCIS), Department of Chemistry, Northwestern University, 2145 Sheridan Road, Evanston, Illinois 60208, United States

[‡]Department of Chemistry, Chemical Theory Center, and Supercomputing Institute, University of Minnesota, 207 Pleasant Street SE, Minneapolis, Minnesota 55455, United States

[§]Chemical Science and Engineering Division, Argonne National Laboratory, 9700 South Cass Avenue, Argonne, Illinois 60439, United States

[∥]School of Chemical Engineering, Purdue University, 480 Stadium Mall Drive, West Lafayette, Indiana 47906, United States

[⊥]X-ray Science Division, Advanced Photon Source, Argonne National Laboratory, Argonne, Illinois 60439, United States

[#]Department of Chemistry, Faculty of Science, King Abdulaziz University, Jeddah 22254, Saudi Arabia

Supporting Information

ABSTRACT: Tandem catalytic systems, often inspired by biological systems, offer many advantages in the formation of highly functionalized small molecules. Herein, a new metal–organic framework (MOF) with porphyrinic struts and Hf_6 nodes is reported. This MOF demonstrates catalytic efficacy in the tandem oxidation and functionalization of styrene utilizing molecular oxygen as a terminal oxidant. The product, a protected 1,2-aminoalcohol, is formed selectively and with high efficiency using this recyclable heterogeneous catalyst. Significantly, the unusual regioselective transformation occurs only when an Fe-decorated Hf_6 node and the Fe–porphyrin strut work in concert. This report is an example of concurrent orthogonal tandem catalysis.

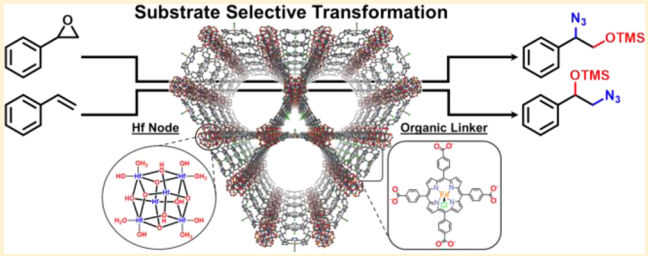

INTRODUCTION

Chemists are often inspired by nature in the pursuit of highly selective architectures when designing new catalysts for chemical transformations. Emergent biological systems often use complex molecular designs and constrained 3D environments to facilitate specific and highly selective chemical transformations as exemplified by catalytically active sites in protein tertiary structures. One approach, mastered by nature, involves the use of a tandem process to increase the synthetic efficiency for specific substrates.[1] Tandem or cascade reactions are extremely valuable processes because reactive intermediates are quickly guided through consecutive reactions toward the desired product. This process essentially eliminates the possibility of product (intermediate) inhibition and slow reaction rates associated with low reactant concentration as well as substrate degradation, while also mitigating side product formation.[2,3]

Metalloporphyrins, a class of metal complexes used ubiquitously in biological systems, have been shown to be essential in many enzymatic processes.[4] Cytochrome P-450 (CP-450) for example, which features an iron porphyrin core, is used extensively in nature to perform catalytic oxidations. The enzymatic pocket of CP-450 protects the porphyrin core and allows for high catalytic turnover, whereas the protein structure provides electrostatic constraints that enhance product selectivity.[5] In a laboratory setting, iron porphyrin is still an active oxidation catalyst, but the absence of a protective protein shell often leads to both catalyst decomposition and non-selective oxidation.[6]

One approach to protecting a catalyst from decomposition involves the incorporation of catalytically active sites within a metal–organic framework (MOF).[7] MOFs are a class of atomically precise and permanently porous materials composed of organic linkers and modular metal clusters.[8] MOFs have been studied for a number of applications including sensing,[9] chemical separations,[10] adsorption, storage and release of gases,[11] light harvesting,[12] and catalysis.[13] Catalysts based on

Received: August 10, 2015
Published: October 4, 2015

DOI: 10.1021/jacs.5b08440
J. Am. Chem. Soc. 2015, 137, 13624–13631

permanently porous MOFs can be utilized to combine the optimal features of homogeneous catalysts (selectivity and ease of modification) and heterogeneous catalysts (ease of purification and recyclability).[14,15] By choosing the appropriate combination of organic linkers and metal clusters, MOFs can be designed to contain catalytically active sites that are uniformly located inside the porous framework.

Recently,[16] we reported a permanently porous Hf-based MOF, Hf-NU-1000, obtained by solvothermal reactive crystallization of $HfOCl_2$, 1,3,6,8-tetrakis(*p*-benzoic acid)pyrene (H_4TBAPy), and benzoic acid as a modulator. Owing to the high density of Lewis acidic sites present within the framework, Hf-NU-1000 was shown to be an excellent catalyst for the regioselective ring opening of styrene oxide, in addition to demonstrating extraordinary chemical stability. Specifically, Hf-NU-1000 allows for the regioselective formation of a protected 1,2-hydroxylamine (**1**) when TMS-N_3 is used to open and trap styrene oxide (Figure 1A).[16] Given that iron porphyrins have been studied extensively for the epoxidation of styrene, we envisioned that a robust MOF consisting of Fe–porphyrin-based struts and catalytically active Hf_6 nodes would give rise to a catalyst capable of performing tandem epoxidation and subsequent epoxide opening. (Figure 1B).

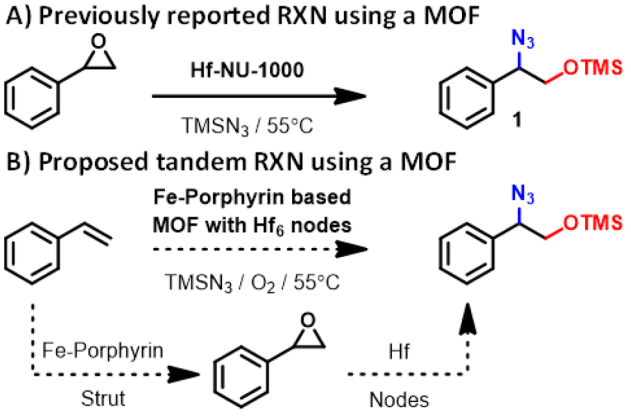

Figure 1. (A) Ring-opening epoxidation using Hf-NU-1000 as a catalyst. (B) Proposed tandem reaction using an Fe–porphyrin, Hf-based MOF to give protected 1,2-hydroxylamine (**1**) in a tandem oxidation/epoxide-opening process.

EXPERIMENTAL SECTION

For detailed experimental procedures including syntheses and characterization data, see the Supporting Information. Briefly, commercial $HfOCl_2 \cdot 8H_2O$ (123 mg, 0.3 mmol), benzoic acid (2.7 g, 22.1 mmol), and *N*,*N*-diethylformamide (DEF, 8 mL) were added to a 20 mL screw-necked glass vial, and the mixture was sonicated to create a fine dispersion. Commercially available *meso*-tetra(4-carboxyphenyl)-porphyrin-Fe(III) chloride (FeTCP-Cl, 53 mg, 0.06 mmol) was added to give a dark-purple suspension. The mixture was placed in a 120 °C oven for 48 h. The reaction vial was removed from the oven and allowed to cool to room temperature. The supernatant was gently decanted, and then fresh *N*,*N*-dimethylformamide (DMF, 20 mL) was added to the vial and shaken. The suspension was transferred to a 50 mL centrifuge vial. The dark (orange under microscope) crystals were isolated by centrifugation, washed five times with fresh DMF (45 mL through repeated centrifugation), and then soaked in fresh DMF (45 mL) for 12 h at 50 °C to wash any unreacted species from the resulting MOF crystals. Then, the dark crystals were isolated by centrifugation, resuspended in acetone (45 mL), and washed five times with fresh acetone (45 mL). Finally, the crystals were soaked in acetone (45 mL) for 12 h for a final rinse. The solid was activated at room temperature under vacuum followed by 120 °C under vacuum for 12 h to yield needlelike crystals with hexagonal faces of Hf-**2** (55 mg, 49% yield).

Hf-**2** single-crystal X-ray diffraction (SC-XRD) data was collected under a cold N_2 gas stream (250 K) on a Bruker Kappa Apex2 diffractometer. Using Olex2,[17] the structure was solved with the ShelXS[18] structure solution program using direct methods and refined with the ShelXL-2014[19] refinement package using least squares minimization. The Supporting Information contains a detailed description of data collection and analysis of structural parameters.

Nitrogen isotherms were recorded on a MicroMeritics ASAP 2020 instrument at 77 K. Detailed experimental procedures for X-ray absorption near-edge structure (XANES), extended X-ray absorption fine structure (EXAFS), and pair distribution functions (PDFs) are described in the Supporting Information.

The metalation of Hf-**2** to give Fe@Hf-**2** is described in section S17 of the Supporting Information. Fe@Hf-**2** has the same structure as Hf-**2** but contains two additional Fe atoms coordinated to the Hf_6 node of the framework to give the overall formula $C_{96}H_{64}Cl_4Fe_4Hf_6N_8O_{32}$. The following is a general procedure for the tandem oxidation reaction using styrene as a substrate and Fe@Hf-**2** as a catalyst. Styrene (23 μL, 0.2 mmol), isobutyraldehyde (36.5 μL, 0.4 mmol), and azidotrimethylsilane (350 μL, 2.6 mmol) were dissolved in acetonitrile (150 μL), and Fe@Hf-**2** (3 mol %, 10 mg) was added to the solution in an autoclave reactor. The autoclave was dried for 6 h at 80 °C prior to addition of reagents. The autoclave reactor was evacuated and purged with O_2, then placed under a constant pressure of O_2 (5 atm gauge pressure) for 10 h during which time it was gently shaken frequently. At the end of the reaction, the reactor was placed in an ice bath for 10 min, and then the vessel was vented and opened. After catalyst separation by centrifugation, a small aliquot of the supernatant reaction mixture was taken to be analyzed by ^1H NMR spectroscopy, in order to calculate the conversion of the reaction. For the recycling experiment, the recovered catalyst was washed with acetonitrile and centrifuged, and the supernatant was decanted. This process was repeated three times; then, the dried catalyst was reused for the next cycle. ***Caution!*** *Azidotrimethylsilane (TMS-N_3) is incompatible with moisture, oxidizing agents, and acids. It is easily decomposed to other compounds, e.g., hydrolyzed to hydrazoic acid (hydrogen azide) which is an extremely toxic and explosive material. Therefore, the safety regulations for this reaction must be followed strictly.*

RESULTS AND DISCUSSION

To test our tandem catalysis hypothesis, we prepared the Fe–porphyrin variant of Hf-NU-1000 (Figure 2). This material is similar in structure to previously prepared PCN-222/MOF-545,[20] an architecture which will be referred to as **2**, consisting of >35 Å hexagonal and 12 Å triangular 1D channels arranged in an alternating manner. Additionally, the metal node, an

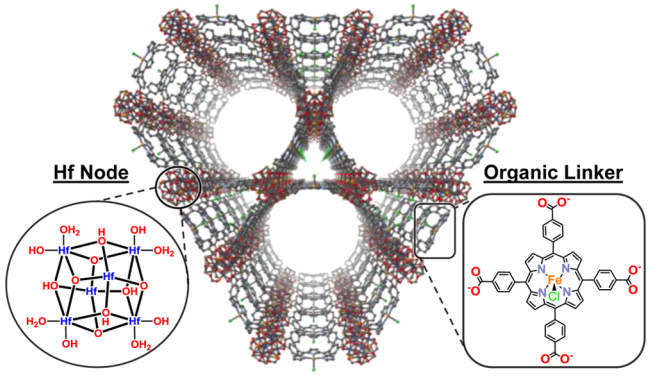

Figure 2. Single-crystal X-ray structure of Hf-**2** highlighting the Hf_6 nodes and the tetracarboxylate Fe–porphyrin linker.

DOI: 10.1021/jacs.5b08440
J. Am. Chem. Soc. 2015, 137, 13624–13631

eight-connected Hf_6-oxo cluster, is identical to the node found in Hf-NU-1000. Single-crystal X-ray analysis (Figure 2) establishes the framework structure and overall topology, whereas powder XRD patterns confirm phase purity of the material (Supporting Information).

As synthesized, each metal node of Hf-**2** contains four additional benzoate ligands as determined by ^{1}H NMR spectroscopy of the digested framework (Supporting Information).[21] The as-synthesized Hf-**2** was studied by N_2 adsorption−desorption experiments at 77 K, and the resulting isotherm (type IVc) yielded a Brunauer−Emmett−Teller (BET) surface area of 1440 m^2 g^{-1} and a total pore volume of 1.03 cm^3 g^{-1}. Initial analysis of the MOF samples showed a lower than expected Fe:Hf ratio[22] (2:6) and therefore in an attempt to ensure that every porphyrin was metalated the as-synthesized Hf-**2** was exposed to a DMF solution containing anhydrous $FeCl_3$. Analysis of the framework after exposure to $FeCl_3$, however, showed removal of ligated benzoic acid molecules, potentially as a result of the in situ generation of HCl, and a further activated framework was obtained.[23] The ^{1}H NMR spectrum (Supporting Information) of the activated Hf-**2** shows a loss of benzoic acid, and the N_2 adsorption−desorption experiments at 77 K indicate an increase in BET surface area to 1600 m^2 g^{-1}. As expected, thermal gravimetric analysis (TGA) of the activated sample displayed no major decomposition up to 450 °C (Supporting Information). Interestingly, inductively coupled plasma (ICP) analysis of the activated material indicates a Fe:Hf ratio of 4:6. This result shows an increase in the amount of Fe incorporated in the framework as compared to that in the as-synthesized MOF, which has an Fe:Hf ratio of only 2:6 (in compliance with the theoretical structural formula with every porphyrin metalated with one Fe atom). The whole number increase of two Fe atoms per node suggests that a well-defined transformation occurs. Diffuse reflectance infrared Fourier transform spectroscopy (DRIFTS) reveals a reduction[24] in intensity of the stretches assigned to terminal −OH groups on the polyhafnium node (Supporting Information), indicating potential functionalization of the free −OH and $-OH_2$ ligands of the Hf nodes.[25] Single-crystal X-ray analysis (Figure 3, close up of the node) of the $FeCl_3$-activated material confirms the presence of Fe atoms coordinated to the Hf_6 node in place of some of the terminal −OH and $-OH_2$ ligands normally present on this eight-connected node. Crystallographically, the data indicate that there are eight locally degenerate positions (Figure 3, circled in orange), which are each 25% occupied, giving a formal two Fe atoms per node.[26] This new, postsynthetically-metalated structure that contains Fe in the porphyrin struts as well as two additional Fe atoms on the Hf_6 nodes will be referred to as Fe@Hf-**2**.

PDF analysis of X-ray total scattering data was used to probe the distribution of Fe ions on the Hf_6-nodes. Differential PDF approaches were applied to isolate the new contributions from atom−atom correlations upon Fe incorporation on the Hf_6-nodes by subtracting the PDF of Hf-**2** (initial framework) from that of Fe@Hf-**2** itself. The experimental differential PDF showed peaks at 3.8, 4.4, and 5.0 Å corresponding to Fe−Hf distances. Simulated PDFs based on single-crystal data indicate three different closest Fe−Hf distances at 3.70, 4.39, and 4.97 Å (Figure 4). Additional peaks were determined at 1.9, 2.9, and 3.2 Å, associated with Fe−O and Fe−Fe, respectively, in agreement with EXAFS analyses. The differential PDF analysis also shows a slight shift of the Hf−O and Hf−Hf peaks, consistent with a cell contraction of the framework.

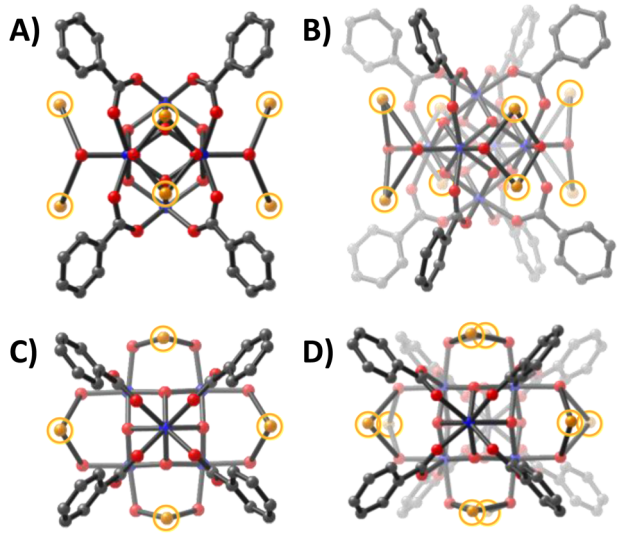

Figure 3. Ball-and-stick representations of the Hf node inside Fe@Hf-**2** viewed along (A) the crystallographic *c* axis, (B) the *abc* plane, (C) the *ab* plane, and (D) the *ab* plane with slight offset. Carbon, oxygen, hafnium, and iron are represented by gray, red, blue, and orange spheres, respectively. The eight symmetry-related positions of the iron atoms are highlighted with orange circles and are 25% occupied to give a total of two iron atoms per node.

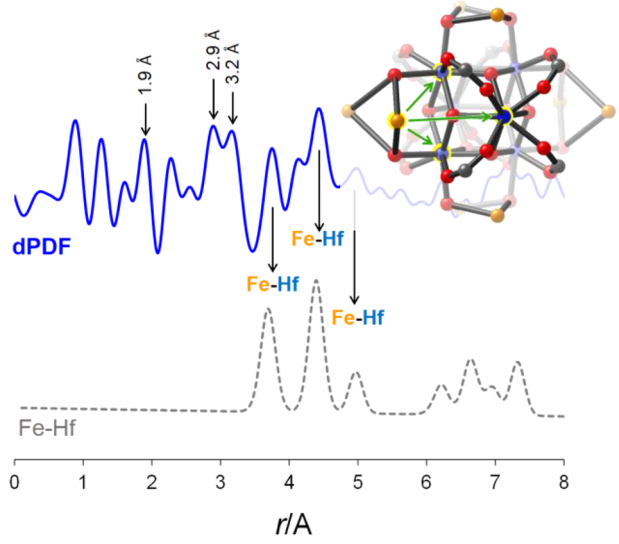

Figure 4. Differential PDFs for Fe@Hf-**2** containing peaks at distances matching the main Fe−Hf interactions at the Hf_6-node.

X-ray absorption spectroscopy measurements were used to gain insight into the oxidation state and coordination environment of Fe present in Fe@Hf-**2**. The Fe K-edge XANES data for Hf-**2**, Fe@Hf-**2**, and FeTCP-Cl is shown in Figure 5. For comparison purposes, $Fe(acac)_3$ and Fe foil were used as references. The position of the pre-K-edge indicates that Fe is present only in a +3 oxidation state,[27] in agreement with XPS data (Supporting Information) of both Hf-**2** and Fe@Hf-**2** as well as in the free Fe(III) porphyrin control (Supporting Information). Figure 6 shows the k^2-weighted χ-function-extended EXAFS spectra for Hf-**2**, Fe@Hf-**2**, and FeTCP-Cl. Because the observed EXAFS spectra are the result of the summation of scattering over all available paths, the EXAFS contribution from the Fe anchored to the node of Fe@

DOI: 10.1021/jacs.5b08440
J. Am. Chem. Soc. 2015, 137, 13624−13631

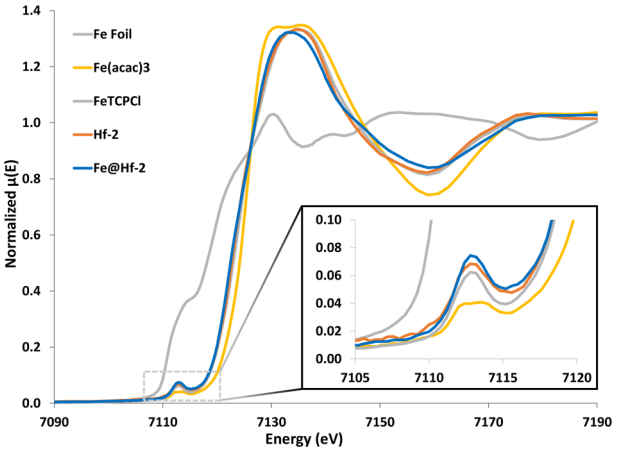

Figure 5. K-edge XANES data of (1) Fe foil, (2) $Fe(acac)_2$, and (3) *meso*-tetra(4-carboxyphenyl)porphyrin-Fe(III)chloride (FeTCP-Cl) as standard, in gray, yellow, and brown, respectively, and the MOF samples (4) Hf-**2** and (5) Fe@Hf-**2** in orange and blue.

Hf-**2** can be isolated if the contribution from the Fe located in the porphyrin of Hf-**2** is known. Because we know that half the Fe in Fe@Hf-**2** resides on the node and the other half is in the porphyrin ring, the data isolation can be achieved using a linear combination of the data from Fe@Hf-**2** with that from either Hf-**2** or FeTCP-Cl as follows:

$$\chi(k)_{obs} = 0.5\chi(k)_{node} + 0.5\chi(k)_{porph} \quad (1)$$

$$\chi(k)_{node} = 2\chi(k)_{obs} - 0.5\chi(k)_{porph} \quad (2)$$

In eqs 1 and 2, $\chi(k)_{obs}$ represents the measured EXAFS spectra, $\chi(k)_{node}$ represents the EXAFS contribution from Fe at the node, and $\chi(k)_{porph}$ represents the EXAFS contribution from Fe in the porphyrin (either in Hf-**2** or FeTCP-Cl). Figure 6B shows the EXAFS spectrum of Fe@Hf-**2** after subtracting contributions from Hf-**2** (blue) and FeTCP-Cl (orange; $\chi(k)_{porph}$, eq 2). The spectra are nearly identical, showing that the Fe porphyrin reference is a good representation of the Fe in the porphyrin struts of the MOF. (See further discussion in the Supporting Information.) The resulting χ-difference spectra can be fit to determine the coordination environment of the Fe on the node. The fit spectra along with experimental data are displayed in Figure 6C–E. The fitting results can be viewed in Table 1. See the Supporting Information for details on the fitting protocol. The XANES and EXAFS data lead us to conclude that in general the nodes of Fe@Hf-**2** contain four

Table 1. EXAFS Fitting Parameters for the Fe–O Scattering Path of Fe on the MOF Node

parameter	value
coordination number (N)	4.39
bond distance (R)	2.00
edge shift (E)	7.42
Debye–Waller factor (σ^2)	0.0046
amplitude reduction Factor (S_o^2)	0.899

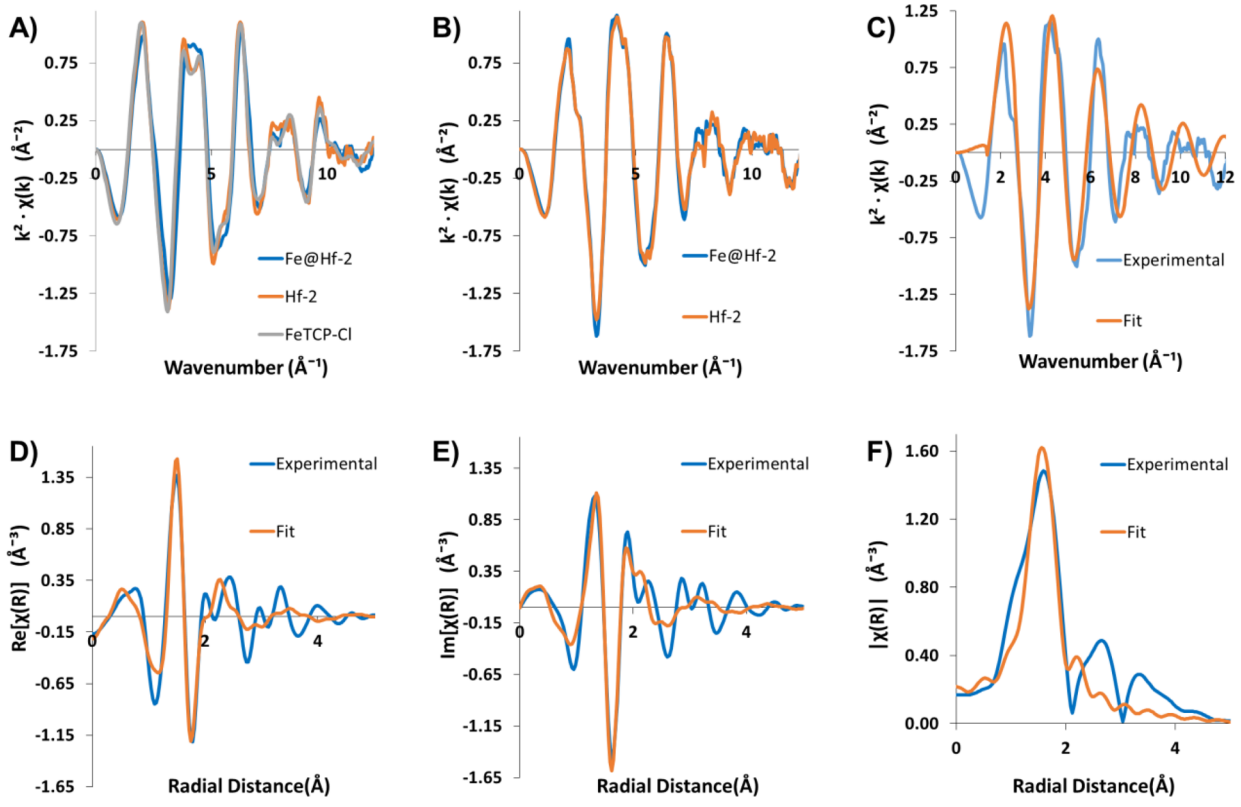

Figure 6. (A) k^2-weighted χ function EXAFS spectra for Fe@Hf-**2**, Hf-**2**, and *meso*-tetra(4-carboxyphenyl)porphyrin-Fe(III)chloride (FeTCP-Cl). (B) k^2-weighted χ function EXAFS spectrum for Fe@Hf-**2** after applying eq 2 to remove any contribution from Hf-**2** (blue) or FeTCP-Cl (orange). Experimental (blue) and fit (orange) data for the Fe@Hf-**2** after subtraction of contributions due to the porphyrin (C) k-space, (D) real part of R-space, (E) imaginary part of R-space, and (F) magnitude of R-space.

DOI: 10.1021/jacs.5b08440
J. Am. Chem. Soc. 2015, 137, 13624–13631

coordinate Fe(III) atoms which could potentially participate in catalytic oxidations.

DFT calculations were carried out to understand more about the coordination of Fe to the Hf_6 node of Hf-**2**. The calculations indicate that the reaction of $FeCl_3$ with the Hf_6 node liberates 2 equiv of HCl and gives rise to a metalated node where Fe(III) is coordinated to one face by three oxygen atoms (one HO bound to Hf, formerly an H_2O and source of one lost proton; one O bound to Hf, formerly an HO and source of one lost proton; and one bridging μ-O atom of the node core) and a remaining Cl (Figure 7A). Further hydrolysis to replace the

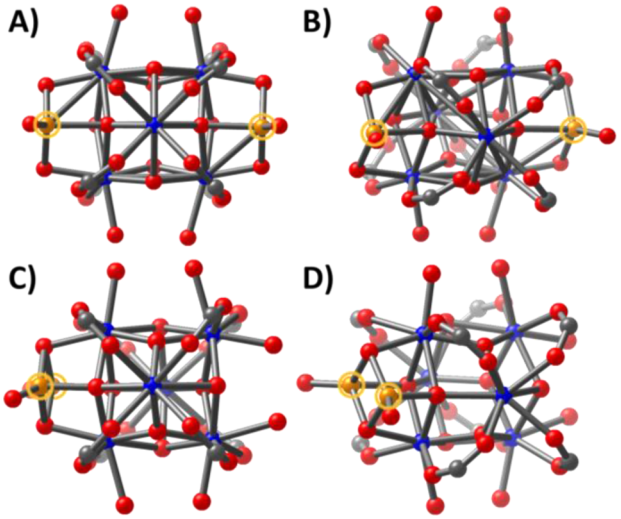

Figure 7. Ball-and-stick representations of (A and B) the lowest computationally determined Hf nodes containing one Fe atom and (C and D) a construct with two bridged Fe atoms on a single face of the Hf node. Carbon, oxygen, hafnium, and iron are represented by gray, red, blue, and orange spheres, respectively. The Fe atoms are highlighted with orange circles for emphasis.

Cl with HO can then take place[28] with the overall tetrahedral, four-coordinate geometry around Fe(III) remaining unchanged. Fe(III) at the Hf_6 node is predicted to be high-spin, which is consistent with the weak ligand-field environment of oxygen. Alternative proton topologies were explored but were found to be higher in energy by 40−70 kJ/mol. Interestingly, coordination of a second Fe(III) was predicted to occur at the same face already decorated with the first Fe(III), proceeding again with loss of 2 equiv of HCl (now coming from the remaining proton on the only HO ligand and the proton on the bridging μ-OH group of the node core), leading to a high-spin ($2S + 1 = 11$) bis-μ-oxo di-iron species (Figure 7B). The separation between the two Fe(III) centers is predicted to be 2.83 Å, which is in good agreement with the observed EXAFS peak at 2.9 Å and also is similar to the distance reported for the first characterized bis-μ-oxo di-iron(III) complex of 2.71 Å. (In the latter case, further coordination by the strong-field tris(6-methylpyridyl-2-methyl)amine ligands lead to a diamagnetic electronic configuration.)[29] Compared to the configuration where the second Fe(III) is placed on the opposite face of the Hf_6node, the bis-μ-oxo dimer is energetically preferred by 57 kJ/mol.

With a new understanding of the location of the additional iron atoms present in Fe@Hf-**2** versus Hf-**2**, the next step was to test the catalytic activity of these new MOFs. Fe@Hf-**2** was indeed found to be catalytically active with full consumption of the starting material in the desired tandem reaction. Under optimized reaction conditions (5 atm O_2, 60 °C, 2.3:1 TMS-N_3/MeCN, 0.4 M, and 2 equiv of *t*-butyraldehyde to regenerate the catalyst), the styrene starting material was completely consumed in 10 h. Surprisingly, the predicted 1,2-hydroxyl amine precursor (**1**) (Figure 1), resulting from opening the postulated styrene oxide intermediate at the thermodynamically favored benzylic carbon atom, was not formed. Instead, a complete reversal in regioselectivity was observed, where the azide reacts (Figure 8) at the kinetically favored terminal

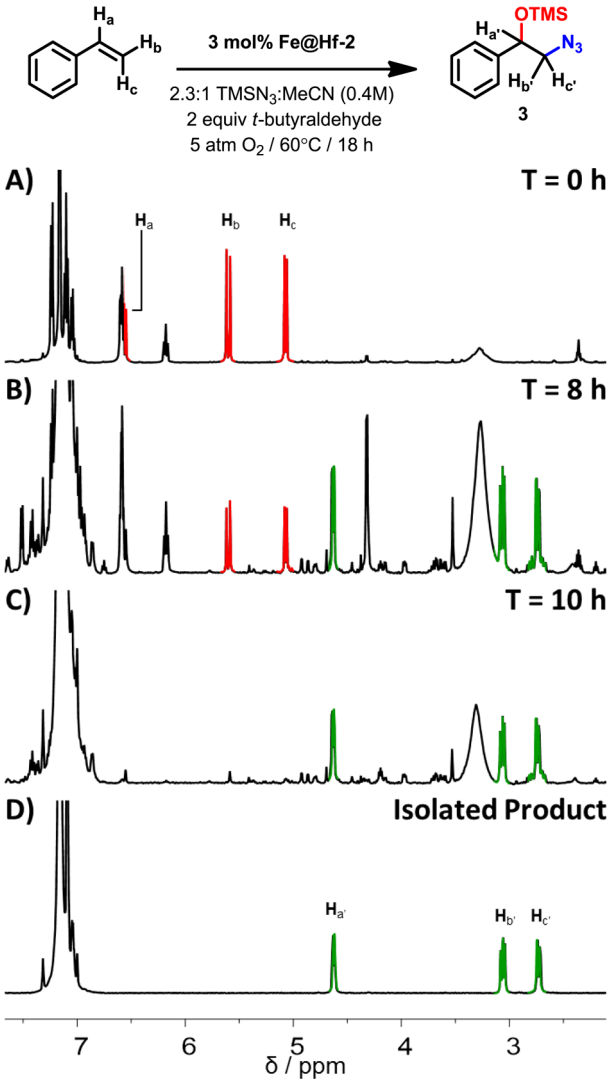

Figure 8. Under the optimized conditions using styrene as substrate, **3** is selectively formed. ^{1}H NMR spectra of the crude reaction mixture at (A) t = 0 h, (B) t = 8 h, and (C) t = 10 h as well as (D) that of the purified product, **3**.

carbon to give the protected 1,2-aminoalcohol (**3**).[30] The overall transformation converts a terminal olefin directly to a protected azidohydrin, which is an important precursor to α-amino alcohols, a common structural motif in biologically relevant molecules such as β-blockers.[31] Indeed, this motif is present in many bioactive natural products,[32] including nucleosides,[33] carbohydrates,[34] oxazolines,[35] and lactams.[36] Azidohydrins, prepared by classic reaction of epoxides with alkali azides are often accompanied by side reactions, such as epimerizations, isomerizations, and rearrangements;[37] only

DOI: 10.1021/jacs.5b08440
J. Am. Chem. Soc. 2015, 137, 13624−13631

recently,[38] the first work showing the selective formation of similar β-azido alcohols using homogeneous metal salts as catalysts[39] was reported.

Numerous control studies were carried out in order to gain a better understanding of the reversal in regioselectivity to give **3** when Fe@Hf-**2** is used as a catalyst. First of all, no leaching of the catalyst was observed during the reaction progress. Additionally, when the same reaction was carried out with Hf-**2**, nonproductive conversion was observed, suggesting that the Fe at the Hf_6 node of Fe@Hf-**2** is playing a significant role in the regioselectivity. When using Hf-NU-1000 with Fe added postsynthetically to the Hf_6 node, however, no reaction takes place, demonstrating that Fe at the node must work in concert with the Fe−porphyrin struts of Fe@Hf-**2** to obtain **3**. Starting from styrene oxide, i.e., the postulated intermediate for this tandem process, under the same reaction conditions and using Fe@Hf-**2** as a catalyst, the thermodynamic product, i.e., regioisomer **1**, was formed (Figure 1). This observation suggests that the reversal in regioselectivity that is observed is governed by the first step of the tandem process.[40] Interestingly, when an Fe-free framework is used as a catalyst under a balloon of oxygen while being irradiated with light, the reaction leads selectively to the originally intended 1,2-hydroxylamine product shown in Figure 1 (Supporting Information), a process which most likely involves the formation of singlet oxygen to promote formation of styrene oxide that can then undergo subsequent ring opening through reaction with the Hf_6 node.[41] These results suggest that a highly selective mode of action is operating for the reaction of styrene inside Fe@Hf-**2** under the original reaction conditions described above.

To probe the potential orthogonal reactivity of styrene and styrene oxide inside Fe@Hf-**2**, we prepared 1,4-di(oxiranyl)-benzene (**4**) and (4-vinylphenyl)oxirane (**5**) as starting materials. Unsurprisingly, **4** was cleanly converted to 1,4-bis(1-azido-2-((trimethylsilyl)oxy)ethyl)benzene (**6**) by nucleophilic azide attack at the thermodynamically favored internal carbon (Figure 9). In stark contrast, **5** reacted (Figure 9) to

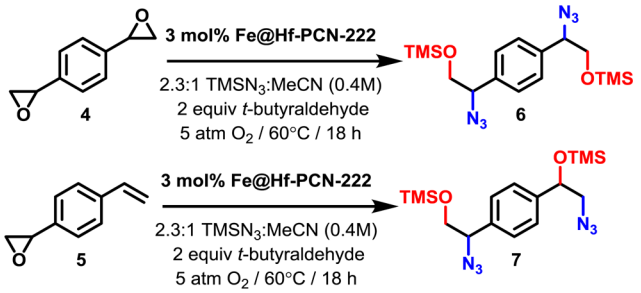

Figure 9. Reactions with **4** and **5** as substrate selectively produced **6** and **7**, respectively, as the major product under the same reaction conditions with Fe@Hf-**2** as the catalyst.

give the mixed product 1-(2′-azido-1′-trimethylsiloxy)-4-(1′-azido-2′-trimethylsiloxy)benzene (**7**). The regioselectivity observed for the products appears to be entirely dependent on the nature of the starting material, further confirming that the reversal in regioselectivity is governed by the first step of the tandem catalytic process.

DFT calculations were carried out to assess the energetics of potential reaction pathways operative in Hf-**2** and Fe@Hf-**2**. When considering the azide opening of styrene oxide, one possible transition state involves coordination of styrene oxide to the Lewis acidic Fe(III)−porphyrin. From this transition state, there is a 25 kJ/mol preference to form the thermodynamically favored regioisomer **1** compared to that for **3**, a prediction which is consistent with the results observed when Fe@Hf-**2** catalyzes the opening of styrene oxide to give **1**. (Much like that for undecorated Hf_6 nodes,[16] complexation to Lewis acidic porphyrin iron favors opening to **1**.) The experimental results suggest that formation of **3** does not proceed via a styrene oxide intermediate but instead by a more complex reaction pathway. One possible mechanism involves an Fe(III)−porphyrin azide intermediate to give an azide radical that can react with styrene and in turn be trapped by peroxycarboxylate, but this pathway entails a very high free energy of activation that is inconsistent with the experimentally observed facile reaction. Cooperativity between two adjacent Fe−porphyrin units, each activated by coordination of an oxo and azido group, was also considered for reaction with styrene; however, the distance between these two units, enforced by the MOF framework, does not allow for this type of cooperativity. Given this information coupled with the experimental results, it seems reasonable to propose that the bis-μ-oxo di-iron functionality on the Hf_6 nodes of Fe@Hf-**2** is responsible for the observed product. Bis-μ-oxo di-iron cores are known to provide a rich environment for oxidation chemistry,[42] and further computational studies are underway to assess possible reaction pathways that take advantage of this iron core.

CONCLUSIONS

The successful use of a heterobimetallic metal−organic framework as a tandem oxidation and trapping catalyst with unexpected selectivity highlights the potential and underexplored reactivity of highly rigid and well-defined heterogeneous catalysts. Taking advantage of the well-ordered and atomically precise construction of metal−organic frameworks will allow chemists to assemble new highly selective catalytic environments. We envisage that further exploration of robust porous coordination networks as easily prepared scaffolds will bring new insight into the fundamental concepts of catalysis.

ASSOCIATED CONTENT

Supporting Information

The Supporting Information is available free of charge on the ACS Publications website at DOI: 10.1021/jacs.5b08440.

Detailed experimental procedures for preparing Hf-**2** and Fe@Hf-**2**, XANES, EXAFS, PDF, single-crystal XRD, DRIFTS, sorption data for the as-synthesized Hf-**2**, activated Hf-**2** and Fe@Hf-**2**, the synthesis of **5**, and general procedure for conducting the tandem reaction. (PDF)

Crystallographic information file for Fe@Hf-**2**. (CIF)

AUTHOR INFORMATION

Corresponding Authors

*E-mail: stoddart@northwestern.edu.
*E-mail: cramer@umn.edu.
*E-mail: j-hupp@northwestern.edu.
*E-mail: o-farha@northwestern.edu

Notes

The authors declare no competing financial interest.

DOI: 10.1021/jacs.5b08440
J. Am. Chem. Soc. 2015, 137, 13624−13631

■ ACKNOWLEDGMENTS

We thank Dr. Ben Klahr for obtaining the SEM images used and the Integrated Molecular Structure Education and Research Center (IMSERC) at Northwestern University for use of its chemical characterization facilities. O.K.F., C.J.C., and J.T.H.: This work (MOF assembly, experimental characterization, catalysis, and modeling) was supported as part of Office of Basic Energy Sciences, Division of Chemical Sciences, Geosciences and Biosciences under Award DE-FG02-12ER16362. J.F.S: This research is part (Project 34-944) of the Joint Center of Excellence in Integrated Nano-Systems (JCIN) at King Abdulaziz City for Science and Technology (KACST) and Northwestern University (NU). Use of the Advanced Photon Source is supported by the U.S. Department of Energy, Office of Science, and Office of Basic Energy Sciences, under Contract DE-AC02-06CH11357. Materials Research Collaborative Access Team (MRCAT, Sectors 10 BM and 10 ID) operations are supported by the Department of Energy and the MRCAT member institutions. J.T.M. and J.R.G. were supported by the U.S. Department of Energy, Office of Basic Energy Sciences, Chemical Sciences under Contract DE-AC-02-06CH11357. We thank both KACST and NU for their continued support of this research. M.H.B. thanks DFG for a Postdoctoral Research Fellowship Award.

■ REFERENCES

(1) Oroz-Guinea, I.; Garcia-Junceda, E. *Curr. Opin. Chem. Biol.* **2013**, *17*, 236−249.

(2) (a) Wasilke, J. C.; Obrey, S. J.; Baker, R. T.; Bazan, G. C. *Chem. Rev.* **2005**, *105*, 1001−1020. (b) Fogg, D. E.; dos Santos, E. N. *Coord. Chem. Rev.* **2004**, *248*, 2365−2379.

(3) A classic biological example of tandem catalysis, i.e., the enzymatic synthesis of L-tryptophan, shows the potential of unique catalysts working together. In this case, the α-subunits of tryptophan synthase catalyze the formation of indole, whereas the β-subunits combine the generated indole with L-serine to complete the synthesis. Within the enzyme, the α and β subunits are held close in space, resulting in a significant increase in the rate of catalysis. One key point to note is that the indole intermediate is not observed in the bulk solution and is instead held near the catalytic site of the enzyme.

(4) Simonneaux, G.; Tagliatesta, P. *J. Porphyrins Phthalocyanines* **2004**, *8*, 1166−1171.

(5) White, R. E. *Science* **1986**, *234*, 884−884.

(6) (a) Bruice, T. C. *Acc. Chem. Res.* **1991**, *24*, 243−249. (b) Groves, J. T. *Nat. Chem.* **2014**, *6*, 89−91. (c) Groves, J. T. In *Cytochrome P450: Structure, Mechanism, and Biochemistry*, 3rd ed.; Ortiz de Montellano, P. R., Ed.; Klewer Academic/Plenum: New York, 2005; pp1−44.

(7) (a) Farha, O. K.; Shultz, A. M.; Sarjeant, A. A.; Nguyen, S. T.; Hupp, J. T. *J. Am. Chem. Soc.* **2011**, *133*, 5652−5655. (b) Gao, W.-Y.; Chrzanowski, M.; Ma, S. *Chem. Soc. Rev.* **2014**, *43*, 5841−5866.

(8) (a) Furukawa, H.; Cordova, K. E.; O'Keeffe, M.; Yaghi, O. M. *Science* **2013**, *341*, 1230444. (b) Gu, Z. Y.; Park, J.; Raiff, A.; Wei, Z. W.; Zhou, H. C. *ChemCatChem* **2014**, *6*, 67−75.

(9) Kreno, L. E.; Leong, K.; Farha, O. K.; Allendorf, M.; Van Duyne, R. P.; Hupp, J. T. *Chem. Rev.* **2012**, *112*, 1105−1125.

(10) (a) Li, J.-R.; Sculley, J.; Zhou, H.-C. *Chem. Rev.* **2012**, *112*, 869−932. (b) Bae, Y.-S.; Hauser, B. G.; Farha, O. K.; Hupp, J. T.; Snurr, R. Q. *Microporous Mesoporous Mater.* **2011**, *141*, 231−235.

(11) (a) Dincă, M.; Long, J. R. *Angew. Chem., Int. Ed.* **2008**, *47*, 6766−6779. (b) Li, J.-R.; Kuppler, R. J.; Zhou, H.-C. *Chem. Soc. Rev.* **2009**, *38*, 1477−1504. (c) Farha, O. K.; Özgür Yazaydın, A.; Eryazici, I.; Malliakas, C. D.; Hauser, B. G.; Kanatzidis, M. G.; Nguyen, S. T.; Snurr, R. Q.; Hupp, J. T. *Nat. Chem.* **2010**, *2*, 944−948.

(12) (a) So, M. C.; Wiederrecht, G. P.; Mondloch, J. E.; Hupp, J. T.; Farha, O. K. *Chem. Commun.* **2015**, *51*, 3501−3510. (b) Kent, C. A.; Liu, D.; Ma, L.; Papanikolas, J. M.; Meyer, T. J.; Lin, W. *J. Am. Chem. Soc.* **2011**, *133*, 12940−12943.

(13) (a) Lee, J.; Farha, O. K.; Roberts, J.; Scheidt, K.; Nguyen, S. T.; Hupp, J. T. *Chem. Soc. Rev.* **2009**, *38*, 1450−1459. (b) Gascon, J.; Corma, A.; Kapteijn, F.; Llabrés i Xamena, F. X. *ACS Catal.* **2014**, *4*, 361−378. (c) Song, F. J.; Wang, C.; Lin, W. B. *Chem. Commun.* **2011**, *47*, 8256−8258. (d) Srirambalaji, R.; Hong, S.; Natarajan, R.; Yoon, M.; Hota, B.; Kim, Y.; Ho Ko, Y.; Kim, K. *Chem. Commun.* **2012**, *48*, 11650−11652.

(14) Climent, M. J.; Corma, A.; Iborra, S.; Sabater, M. J. *ACS Catal.* **2014**, *4*, 870−891.

(15) (a) Liu, J.; Chen, L.; Cui, H.; Zhang, J.; Zhang, L.; Su, C.-Y. *Chem. Soc. Rev.* **2014**, *43*, 6011−6061. (b) Ma, L. Q.; Abney, C.; Lin, W. B. *Chem. Soc. Rev.* **2009**, *38*, 1248−1256. (c) Gao, W. Y.; Chrzanowski, M.; Ma, S. Q. *Chem. Soc. Rev.* **2014**, *43*, 5841−5866.

(16) Beyzavi, M. H.; Klet, R. C.; Tussupbayev, S.; Borycz, J.; Vermeulen, N. A.; Cramer, C. J.; Stoddart, J. F.; Hupp, J. T.; Farha, O. K. *J. Am. Chem. Soc.* **2014**, *136*, 15861−15864.

(17) Dolomanov, O. V.; Bourhis, L. J.; Gildea, R. J.; Howard, J. A. K.; Puschmann, H. J. *J. Appl. Crystallogr.* **2009**, *42*, 339−341.

(18) Sheldrick, G. M. *Acta Crystallogr., Sect. A: Found. Crystallogr.* **2008**, *64*, 112−122.

(19) Sheldrick, G. M. *Acta Crystallogr., Sect. A: Found. Adv.* **2015**, *71*, 3−8.

(20) (a) Feng, D.; Gu, Z.-Y.; Li, J.-R.; Jiang, H.-L.; Wei, Z.; Zhou, H.-C. *Angew. Chem., Int. Ed.* **2012**, *51*, 10307−10310. (b) Morris, W.; Volosskiy, B.; Demir, S.; Gándara, F.; McGrier, P. L.; Furukawa, H.; Cascio, D.; Stoddart, J. F.; Yaghi, O. M. *Inorg. Chem.* **2012**, *51*, 6443−6445.

(21) At this time, the specific location of each additional benzoic acid molecule in the as-synthesized Hf-**1**, Hf-NU-1000, NU-1000, or PCN-222/MOF-545 frameworks should be similar to what we published previously. See Deria, P.; Mondloch, J. E.; Tylianakis, E.; Ghosh, P.; Bury, W.; Snurr, R. Q.; Hupp, J. T.; Farha, O. K. *J. Am. Chem. Soc.* **2013**, *135*, 16801−16804. Deria, P.; Bury, W.; Hupp, J. T.; Farha, O. K. *Chem. Commun.* **2014**, *50*, 1965−1968. In our hands, each attempt at preparing the aforementioned structures results in the inclusion of exactly four benzoic acid molecules per node, as determined by comparing the ratio of benzoic acid and the tetra-acid linker using ^{1}H NMR spectroscopy, and leads us to conclude that the node is responsible for the accumulated benzoic acids. Looking at the crystal structure of NU-1000, we envision that four benzoates could function as ligands to the four most exposed metal atoms on the node, pointing the aromatic ring into the large hexagonal pore of the framework.

(22) After further investigation, it was found that the low Fe/Hf ratio was a consequence of a mathematical error and that the as-synthesized material was in fact fully metalated.

(23) To activate Hf-**2** toward catalysis, $FeCl_3$ was used to ensure complete metalation of the porphyrin functionality. The in situ generated HCl provides an acidic environment able to cleave the benzoate ligands occupying the nonstructural coordination sites on the polyoxo-hafnium nodes.

(24) The DRIFTS experiments were compared to Hf-**2** that was activated with HCl to remove all the benzoic acid from the nodes. The HCl-treated Hf-**2** shows the same 2:6 Fe/Hf ratio as the as-synthesized material, whereas ^{1}H NMR spectroscopy shows the complete removal of exogenous benzoic acid molecules.

(25) Planas, N.; Mondloch, J. E.; Tussupbayev, S.; Borycz, J.; Gagliardi, L.; Hupp, J. T.; Farha, O. K.; Cramer, C. J. *J. Phys. Chem. Lett.* **2014**, *5*, 3716−3723.

(26) The crystal structure of Fe@Hf-**2** has been uploaded to the Cambridge Crystallographic Data Centre (CCDC 1418428).

(27) Krogman, J. P.; Gallagher, J. R.; Zhang, G.; Hock, A. S.; Miller, J. T.; Thomas, C. M. *Dalton Trans.* **2014**, *43*, 13852−13857.

(28) Elemental analysis carried out on Fe@Hf-**2** indicates that no additional Cl is incorporated into the structure as compared to the structure of Hf-**2**. It is reasonable that the $FeCl_3$ incorporated into the framework can be hydrolyzed to produce Fe oxides attached to the Hf nodes.

DOI: 10.1021/jacs.5b08440
J. Am. Chem. Soc. 2015, 137, 13624−13631

(29) Zang, Y.; Dong, Y.; Que, L., Jr.; Kauffmann, K.; Muenck, E. *J. Am. Chem. Soc.* **1995**, *117*, 1169−1170.
(30) An NMR yield of 53% for **3** was determined using 1,4-bis(trifluoromethyl)bezene as an internal standard.
(31) Tae Cho, B.; Kyu Kang, S.; Hye Shin, S. *Tetrahedron: Asymmetry* **2002**, *13*, 1209−1217.
(32) Smith, J. G. *Synthesis-Stuttgart* **1984**, *10*, 629−656.
(33) Coe, D. M.; Myers, P. L.; Parry, D. M.; Roberts, S. M.; Storerb, R. *J. Chem. Soc., Chem. Commun.* **1990**, 151−153.
(34) Scriven, E. F. V.; Turnbull, K. *Chem. Rev.* **1988**, *88*, 297−368.
(35) Badiang, J. G.; Aube, J. *J. Org. Chem.* **1996**, *61*, 2484−2487.
(36) Smith, B. T.; Gracias, V.; Aube, J. *J. Org. Chem.* **2000**, *65*, 3771−3774.
(37) *The Chemistry of the Azido Group*; Patai, S., Ed.; The Chemistry of Functional Groups Series; Wiley: London, 1971.
(38) Sun, X.; Li, X.; Song, S.; Zhu, Y.; Liang, Y.-F.; Jiao, N. *J. Am. Chem. Soc.* **2015**, *137*, 6059−6066.
(39) Kas'yan, L. I.; Okovityi, S. I.; Kas'yan, A. O. *Russ. J. Org. Chem.* **2004**, *40*, 1−34.
(40) Other control studies carried out include the homogeneous reaction of styrene with Fe(III)*meso*-tetra(4-carboxyphenyl)porphine chloride tetramethyl ester, resulting in the formation of only a small amount of styrene oxide and benzaldehyde. In addition, if the reaction is carried out in the absence of $TMSN_3$, then no reaction is observed.
(41) Liu, Y.; Howarth, A. J.; Hupp, J. T.; Farha, O. K. *Angew. Chem., Int. Ed.* **2015**, *54*, 9001−9005.
(42) (a) Que, L., Jr.; Tolman, W. B. *Angew. Chem., Int. Ed.* **2002**, *41*, 1114−1137. (b) Friedle, S.; Reisner, E.; Lippard, S. J. *Chem. Soc. Rev.* **2010**, *39*, 2768−2779.

DOI: 10.1021/jacs.5b08440
J. Am. Chem. Soc. 2015, 137, 13624−13631